

INITIATION AND EVOLUTION OF GLOBAL CORONAL WAVES

B. VRŠNAK¹, N. MUHR², T. ŽIC¹, S. LULIĆ³,
I. W. KIENREICH², M. TEMMER², A. M. VERONIG².

¹*Hvar Observatory, Faculty of Geodesy, Kačićeva 26,
HR-10000 Zagreb, Croatia*

²*Institute of Physics, University of Graz, Universitätsplatz 5,
A-8010 Graz, Austria*

³*Karlovac University of Applied Sciences, Trg J.J.Strossmayera 9,
HR-47000 Karlovac, Croatia*

Abstract. Some essential outcomes of a detailed analysis of the formation and evolution of the coronal EUV wave of 15 February 2011 are presented, focused on the relationship between the source region expansion, wave kinematics, and the evolution of the wave amplitude. The observations are explained in terms of the results of the numerical MHD simulations, providing new insights into the physical background of coronal waves, especially considering the nature of the relationship of the wave amplitude and propagation velocity in different phases of the wave evolution.

Key words: coronal EUV waves, Moreton waves, coronal mass ejections, flares

1. Introduction

Large-amplitude global coronal waves, caused by solar coronal eruptions, were in focus of numerous empirical and theoretical studies in the past decade (see reviews by Warmuth, 2007; Vršnak and Cliver, 2008; Wills-Davey and Attrill, 2009; Warmuth, 2010; Gallagher and Long, 2011; Zhukov, 2011; Patsourakos and Vourlidas, 2012; Liu and Ofman, 2014). In this paper we report some preliminary results of a study that follows up our previous theoretical research on this phenomenon (Vršnak and Lulić, 2000a,b; Žic *et al.*, 2008; Lulić *et al.*, 2013). It is directly related to the empirical research performed in the scope of the very fruitful long-lasting “Graz-Hvar” collaboration in studying the nature of large-amplitude global coronal MHD waves and shocks (Balasubramaniam *et al.*, 2010; Kienreich *et al.*, 2009,

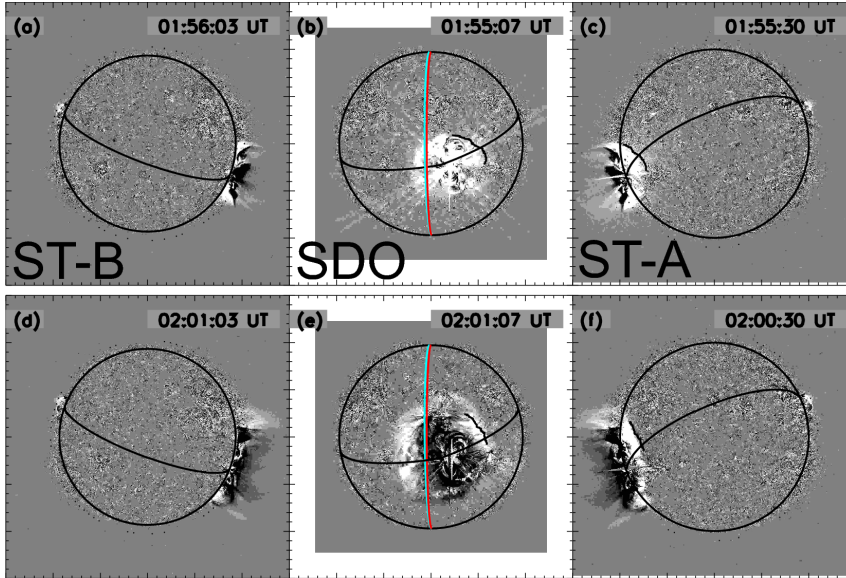


Figure 1: Running difference images of STEREO/EUVI-B and -A 195 \AA (left and right, respectively) and SDO/AIA 193 \AA (middle). The black lines indicate great circles starting at the determined wave-source center in the measured propagation directions. The red and blue lines in SDO images represent the ST-A and ST-B limb, respectively, whereas the hand-drawn lines are the fronts transposed from the ST-A and ST-B images.

2011, 2013; Muhr *et al.*, 2008, 2010, 2011, 2014; Temmer *et al.*, 2009, 2013; Veronig *et al.*, 2006, 2008, 2010, 2011; Vršnak *et al.*, 2002, 2005, 2006; Warmuth *et al.*, 2001, 2004a,b). The paper concerns the formation and evolution of the coronal waves, particularly focusing on the relationship between the source region expansion, wave kinematics, and the evolution of the wave amplitude. First, we present some essential outcomes of a detailed analysis of the coronal EUV wave of 15 February 2011 (Section 2), which are then explained employing numerical MHD modeling (Section 3) to provide new insights into the nature of coronal waves.

2. Observations

The coronal EUV wave under study was caused by the eruption of the coronal mass ejection (CME) and the associated X2.2 flare that started around 01:45 UT on 15 February 2011. The event was observed from three view-

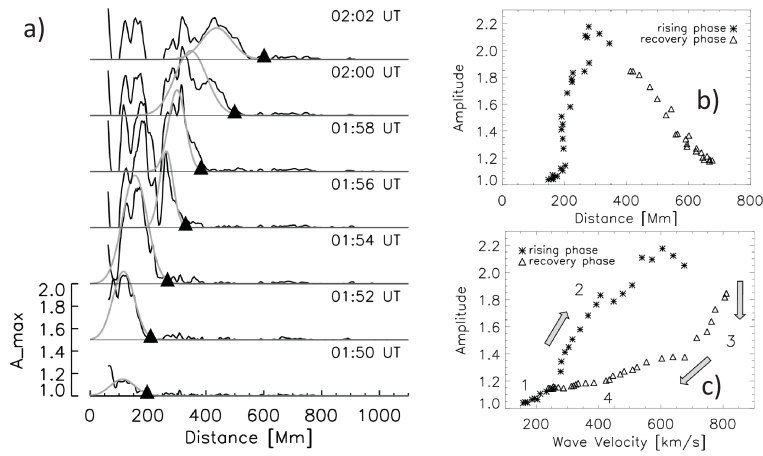


Figure 2: a) SDO/AIA 211 Å perturbation profiles. The triangles indicate the leading edge of the EUV wave front positions as derived by the Gaussian fits (grey curves) at the 2% level above background. b) Amplitude of the perturbation profile against the distance. c) Velocity of the EUV wave derived from AIA 211 Å observations during 01:48 UT-02:12 UT. Arrows indicate the temporal evolution along the loop.

points by AIA/SDO and EUVI/STEREO-A&B, providing a very detailed insight into its evolution. The initiation of this EUV wave was studied by Schrijver *et al.* (2011), whereas Olmedo *et al.* (2012) analyzed the “reflection” from, and “transmission” through, a coronal hole. Figure 1 depicts the evolution of the wave. The wave propagation was measured by the perturbation-profile method proposed by Muhr *et al.* (2011), the visual-tracking method, and the stack-plot method. In Figure 2a the application of the perturbation-profile method is illustrated. The behavior of the EUV-wave amplitude, determined from gaussian fits like those shown in Figure 2a, is displayed in Figure 2b. The evolution of the wave in the amplitude-velocity space is shown in Figure 2c, revealing a hysteresis-like behavior, analogous to that spotted in the numerical simulations by Lulić *et al.* (2013).

In Figure 3 the evolution of the wave speed and amplitude (the ratio of the wave intensity and the pre-event coronal intensity) is compared with the evolution of the CME velocity and the flare X-ray burst. The first vertical line at 01:55 UT marks the EUV-wave peak amplitude, which is simultaneous with the CME peak acceleration and the X-ray burst maximum. The second vertical line at 01:59 UT indicates the EUV-wave peak velocity,

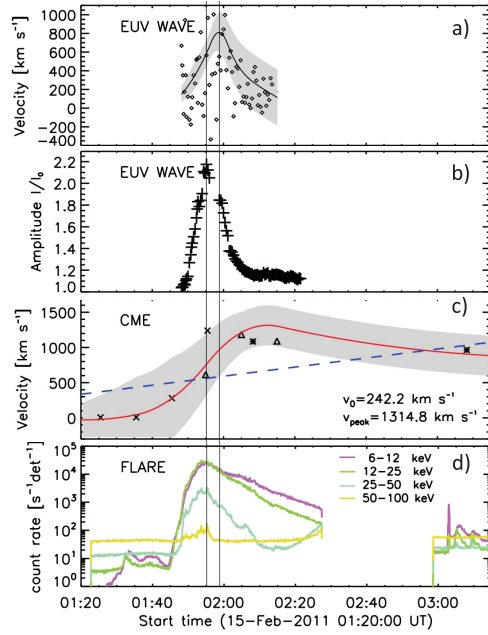


Figure 3: Evolution of: a) wave velocity; b) wave amplitude; c) CME velocity d) RHESSI soft and hard X-ray flux. Note that the fastest growth of the CME speed occurs at the time of the X-ray burst peak.

which is delayed after the peak amplitude by 4 min. In the first stage the EUV wave accelerates from ≈ 200 to a maximum speed of $\approx 800 \text{ km s}^{-1}$, reached at $\approx 01:59 \text{ UT}$ ($a = 900 \text{ m s}^{-2}$). Thereafter, the wave decelerates back to $\approx 200 \text{ km s}^{-1}$ ($a = -750 \text{ m s}^{-2}$). The wave amplitude changes from ≈ 1 to a maximum value of ≈ 2 in the period 01:48–01:55 UT, corresponding to the flare impulsive phase characterized by the hard X-ray burst, i.e., the rising phase of the soft X-ray burst. The understanding of the evolution of the wave speed and amplitude in the context of different stages of the CME/flare-eruption, and the explanation of the “hysteresis” signature, is the main objective of Section 3.

3. Numerical simulations

To get a deeper insight into the wave behavior described in Section 2, we analyze quantitatively the outcome of the numerical simulations performed

by employing the *Versatile Advection Code* (VAC; Tóth, 1996; Goedbloed *et al.*, 2003, for a brief overview see Lulić *et al.*, 2013). In the simulation, the coronal wave is launched by the eruption of an unstable upward-propagating radially-expanding flux-rope. All quantities in the simulation are dimensionless, so that the numerical box has length $L = 1$, the velocities are normalized with respect to the background Alfvén speed, $v_A = 1$, and the time is expressed in the units of the Alfvén travel time across the numerical box, $t_A = L/v_A$. The field lines overlying the flux-rope are anchored in the chromosphere that extends up to $y = 0.1$. The background magnetic field is set up in such a way that roughly reproduce to the helmet-streamer arcade that embeds the flux-rope. It consists of vertical field of opposite orientation on opposite sides of the rope and the poloidal component due to the current flowing along the rope.

In Figure 4a two snapshots of the simulated evolution of the system are shown. The inner region of increased density represents the flux rope, and the outer shell in the right panel corresponds to the sheath region behind the wavefront. The vertical thin region of increased density above the flux rope represents the helmet-streamer current sheet. At $t = 0$ the flux-rope center is set at $y = 0.2$ and the whole rope moves upward at a speed of $v = 1$.

The evolution of the density profiles along the $y = 0.2$ layer is presented in Figure 4b. The two sharp density peaks that slowly expand outwards from $x = \pm 0.1$ represent the outermost shell of the flux-rope (“contact surface”; “piston”), where the plasma piles up due to lateral expansion of the rope. The density within the rope decreases in time, corresponding to the CME core-dimming. Ahead of the contact surface the wave forms (left panel – formation phase; right panel – propagation phase). At a certain time, a density depletion forms in the wake of the wavefront, corresponding to the transient coronal dimming propagating behind the EUV wave.

In Figure 4c the evolution of various features is quantified, based on the simulation results is presented. In the left panel we display as a function of time the piston velocity, v_p , the wave phase velocity, w , and the wave-crest amplitude, X . In the right panel the evolution of the wave is presented in the wave velocity-amplitude space, $w(X)$. The arrows indicate the sense of the “motion” of the system along the displayed evolutionary loop.

Figure 3 reveals that the wave amplitude and speed in the event under study occur after the the strongest energy release in the associated flare and

the highest acceleration of the CME. The latter is opposite to the simulation, where the piston achieves maximum speed before the wave (Figure 4c-left). This implies that the low-height lateral expansion of the CME, responsible for the EUV wave formation, must have achieved maximum speed before the CME forehead does (for such a behavior see Vršnak *et al.*, 2004; Maričić *et al.*, 2004).

Note that in Figure 4c-right the sense of the temporal evolution along the speed-amplitude loop is oriented in the opposite direction than in the “hysteresis” shown in Figure 3c. In this respect it should be emphasized that in Figure 6 of Lulić *et al.* (2013), where the simulation of the flux-rope expansion in a homogeneous medium was treated, the sense of the evolutionary loop was consistent with Figure 3c. On the other hand, in the simulation presented in this paper the magnetic field strength and the Alfvén speed decrease with distance from the flux-rope.

In the simulations presented in this paper, as well as in Lulić *et al.* (2013), the wave amplitude and the wave speed increase during the driven phase (expanding piston). The difference appears in the propagation phase, which corresponds to the deceleration and retreat of the piston. In the simulation presented by Lulić *et al.* (2013) the ambient Alfvén speed is constant, so both the wave amplitude and the wave speed decrease due to the radial expansion of the wavefront (conservation of the energy flux). Thus, after the wave growth and acceleration, the amplitude achieves maximum before the wave speed does, i.e., it already decreases during the maximum-speed phase (like in the observations presented in Section 2; see Figure 3). Eventually, both the wave amplitude and the wave speed decrease.

On the other hand, since in the simulation employed in this paper the ambient Alfvén speed decreases with distance, beside the effect of the radial expansion, the so-called “signal pile-up” phenomenon affects the wave evolution too. The latter effect means that the wave amplitude and the Mach number tend to increase, whereas the phase speed should decrease due to the background Alfvén speed decrease. Since the rate at which the Alfvén speed decreases is progressively diminishing with the distance, i.e., the slope of $v_A(x)$ is less and less steep, the “pile-up” effect is dominant only at the beginning of the wave evolution, so eventually the effect of the radial expansion becomes dominant.

Consequently, the wave amplitude achieves maximum before the wave speed, i.e., the wave speed already decreases while the amplitude still in-

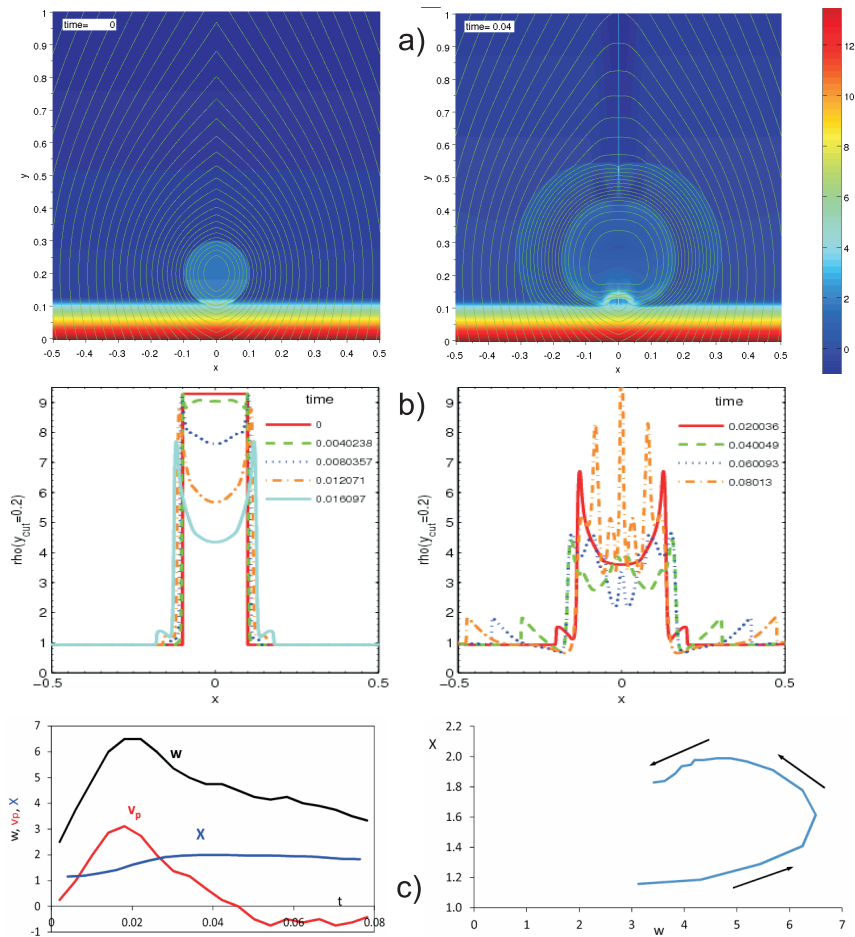


Figure 4: a) Snapshots of the simulated eruption at $t = 0$ (left) and $t = 0.04$ (right) Magnetic field lines are drawn in white. The density is color-coded. b) Density profiles at different times (written in the inset); left – wave-growth phase, right – propagation phase. c) Left: Evolution of the wave phase velocity (w ; black), the piston velocity (v_p ; red), and the density amplitude (X ; blue); Right: Density amplitude versus the wave phase velocity (arrows indicate the temporal evolution).

creases, which makes the sense of the temporal evolution in the velocity-amplitude loop to be opposite compared to the case of a constant Alfvén speed. The sense of the evolution along the velocity-amplitude loop, which is consistent with the constant Alfvén speed case (compare Figure 2c of this paper with Figure 6 in the paper by Lulić *et al.*, 2013), implies that the observed deceleration of the wave is a direct consequence of the radial expansion of the wavefront, i.e., it is not caused by the decrease of the Alfvén speed with distance from the active region, as somebody might conclude from Figures 10 and 11 of Warmuth and Mann (2005).

4. Conclusion

In this paper we have demonstrated how important it is to perform a very careful comparison of observations/measurements with a detailed quantitative analysis of numerical simulations in getting a deeper physical comprehension of the nature of coronal EUV waves. Moreover, such an approach is also essential for reliable estimates of various coronal parameters (e.g., Alfvén speed, magnetic field, etc.) when characteristics of different signatures of global coronal waves and shocks (e.g., EUV waves, radio type II bursts, Moreton waves, etc.) are used for the coronal-diagnostics purposes. As we have demonstrated in the presented study, in this respect particularly important is the behavior of the evolutionary “hysteresis loop” of the amplitude–velocity relationship.

Acknowledgements

B.V. and T.Ž. acknowledge financial support by Croatian Science Foundation under the project 6212 “Solar and Stellar Variability” (SOLSTEL). N.M., I.W.K., M.T., and A.M.V. acknowledge the Austrian Science Fund (FWF): P20867-N16, P-24092-N16, and V195-N16. N.M. acknowledges the MOEL-Plus Förderprogramm. The Versatile Advection Code (VAC) was developed by Gábor Tóth at the Astronomical Institute at Utrecht, in a collaboration with the FOM Institute for Plasma Physics, the Mathematics department at Utrecht and the CWI at Amsterdam.

References

- Balasubramaniam, K. S., Cliver, E. W., Pevtsov, A., Temmer, M., Henry, T. W., Hudson, H. S., Imada, S., Ling, A. G., Moore, R. L., Muhr, N., Neidig, D. F., Petrie, G. J. D., Veronig, A. M., Vršnak, B., and White, S. M.: 2010, *Astrophys. J.* **723**, 587–601.
- Gallagher, P. T. and Long, D. M.: 2011, *Space Sci. Rev.* **158**, 365–396.
- Goedbloed, J. P., Keppens, R., and Poedts, S.: 2003, *Space Sci. Rev.* **107**, 63–80.
- Kienreich, I. W., Muhr, N., Veronig, A. M., Berghmans, D., De Groof, A., Temmer, M., Vršnak, B., and Seaton, D. B.: 2013, *Sol. Phys.* **286**, 201–219.
- Kienreich, I. W., Temmer, M., and Veronig, A. M.: 2009, *Astrophys. J., Lett.* **703**, L118–L122.
- Kienreich, I. W., Veronig, A. M., Muhr, N., Temmer, M., Vršnak, B., and Nitta, N.: 2011, *Astrophys. J., Lett.* **727**, L43.
- Liu, W. and Ofman, L.: 2014, *Sol. Phys.* **289**, 3233–3277.
- Lulić, S., Vršnak, B., Žic, T., Kienreich, I. W., Muhr, N., Temmer, M., and Veronig, A. M.: 2013, *Sol. Phys.* **286**, 509–528.
- Maričić, D., Vršnak, B., Stanger, A. L., and Veronig, A.: 2004, *Sol. Phys.* **225**, 337–353.
- Muhr, N., Temmer, M., Veronig, A., Vršnak, B., and Hanslmeier, A.: 2008, *Centr. Europ. Astrophys. Bull.* **32**, in press.
- Muhr, N., Veronig, A. M., Kienreich, I. W., Temmer, M., and Vršnak, B.: 2011, *Astrophys. J.* **739**, 89.
- Muhr, N., Veronig, A. M., Kienreich, I. W., Vršnak, B., Temmer, M., and Bein, B. M.: 2014, *Sol. Phys.* **289**, 4563–4588.
- Muhr, N., Vršnak, B., Temmer, M., Veronig, A. M., and Magdalenic, J.: 2010, *Astrophys. J.* **708**, 1639–1649.
- Olmedo, O., Vourlidas, A., Zhang, J., and Cheng, X.: 2012, *Astrophys. J.* **756**, 143.
- Patsourakos, S. and Vourlidas, A.: 2012, *Sol. Phys.* **281**, 187–222.
- Schrijver, C. J., Aulanier, G., Title, A. M., Pariat, E., and Delannée, C.: 2011, *Astrophys. J.* **738**, 167.
- Temmer, M., Vršnak, B., Žic, T., and Veronig, A. M.: 2009, *Astrophys. J.* **702**, 1343–1352.
- Temmer, M., Vršnak, B., and Veronig, A. M.: 2013, *Sol. Phys.* p. tmp194.
- Tóth, G.: 1996, *Astrophys. Lett. Comm.* **34**, 245–250.
- Veronig, A. M., Gömöry, P., Kienreich, I. W., Muhr, N., Vršnak, B., Temmer, M., and Warren, H. P.: 2011, *Astrophys. J., Lett.* **743**, L10.
- Veronig, A. M., Muhr, N., Kienreich, I. W., Temmer, M., and Vršnak, B.: 2010, *Astrophys. J., Lett.* **716**, L57–L62.

- Veronig, A. M., Temmer, M., and Vršnak, B.: 2008, *Astrophys. J., Lett.* **681**, L113–L116.
- Veronig, A. M., Temmer, M., Vršnak, B., and Thalmann, J. K.: 2006, *Astrophys. J.* **647**, 1466–1471.
- Vršnak, B. and Cliver, E. W.: 2008, *Sol. Phys.* **253**, 215–235.
- Vršnak, B. and Lulić, S.: 2000a, *Sol. Phys.* **196**, 157–180.
- Vršnak, B. and Lulić, S.: 2000b, *Sol. Phys.* **196**, 181–197.
- Vršnak, B., Magdalenić, J., Temmer, M., and Veronig, A. , *et al.*: 2005, *Astrophys. J.* **625**, L67–L70.
- Vršnak, B., Maričić, D., Stanger, A. L., and Veronig, A.: 2004, *Sol. Phys.* **225**, 355–378.
- Vršnak, B., Warmuth, A., Brajša, R., and Hanslmeier, A.: 2002, *Astron. Astrophys.* **394**, 299–310.
- Vršnak, B., Warmuth, A., Temmer, M., Veronig, A., Magdalenić, J., Hillaris, A., and Karlický, M.: 2006, *Astron. Astrophys.* **448**, 739–752.
- Warmuth, A.: 2007, in K.-L. Klein and A. L. MacKinnon (eds), *Lecture Notes in Physics*, Springer Verlag, Berlin, , Vol. 725, pp. 107–138.
- Warmuth, A.: 2010, *Adv. Space Res.* **45**, 527–536.
- Warmuth, A. and Mann, G.: 2005, *Astron. Astrophys.* **435**, 1123–1135.
- Warmuth, A., Vršnak, B., Magdalenić, J., Hanslmeier, A., and Otruba, W.: 2004a, *Astron. Astrophys.* **418**, 1101–1115.
- Warmuth, A., Vršnak, B., Magdalenić, J., Hanslmeier, A., and Otruba, W.: 2004b, *Astron. Astrophys.* **418**, 1117–1129.
- Warmuth, A., Vršnak, B., Aurass, H., and Hanslmeier, A.: 2001, *Astrophys. J.* **560**, L105–L109.
- Wills-Davey, M. J. and Attrill, G. D. R.: 2009, *Space Sci. Rev.* **149**, 325–353.
- Zhukov, A. N.: 2011, *J. Atmo. Solar-Terr. Phys.* **73**, 1096–1116.
- Žic, T., Vršnak, B., Temmer, M., and Jacobs, C.: 2008, *Sol. Phys.* **253**, 73–83.